HHS Public Access

Author manuscript

Neuron. Author manuscript; available in PMC 2019 March 21.

Published in final edited form as:

Neuron. 2018 March 21; 97(6): 1369–1381.e5. doi:10.1016/j.neuron.2018.01.049.

Activation of striatal neurons causes a perceptual decision bias during visual change detection in mice

Lupeng Wang[1], **Krsna V. Rangarajan**[1], **Charles R. Gerfen**[2], and **Richard J. Krauzlis**[1]

[1]Laboratory of Sensorimotor Research, National Eye Institute Bethesda, Maryland 20892 USA

[2]Laboratory of Systems Neuroscience, National Institute of Mental Health Bethesda, Maryland 20892 USA

Summary

The basal ganglia are implicated in perceptual decision-making, although their specific contributions remain unclear. Here we tested the causal role of the basal ganglia by manipulating neuronal activity in the dorsal striatum of mice performing a visual orientation-change detection (yes/no) task. Brief unilateral optogenetic stimulation caused large changes in task performance, shifting psychometric curves upward by increasing the probability of "yes" responses with only minor changes in sensitivity. For the direct pathway, these effects were significantly larger when the visual event was expected in the contralateral visual field, demonstrating a lateralized bias in responding to sensory inputs rather than a generalized increase in action initiation. For both direct and indirect pathways, the effects were specific to task epochs in which choice-relevant visual stimuli were present. These results indicate that the causal link between striatal activity and decision-making includes an additive perceptual bias in favor of expected or valued visual events.

eTOC Blurb

Using a visual change detection task in mice, Wang et al. demonstrate that the direct and indirect pathways in the basal ganglia contribute to perceptual decision-making by biasing choices in favor of expected or valued visual events.

Introduction

The basal ganglia are a set of subcortical nuclei that play a central role in regulating actions (Dudman and Krakauer, 2016; Hikosaka et al., 2014). The complete basal ganglia circuit is astonishingly complex, but the basic backbone is well established. The striatum, the main

Corresponding Author & Lead Contact: Richard J. Krauzlis, richard.krauzlis@nih.gov.

Author Contributions

L.W. and R.J.K designed the experiments and wrote the manuscript. L.W. and K.V.R. trained the mice, and L.W. conducted the experiments. L.W., C.R.G and R.J.K. analysed the data.

Declaration of Interests

The authors declare no competing interests.

input nucleus of the basal ganglia, contains distinct classes of projection neurons that give rise to pathways with complementary roles – a direct pathway through the substantia nigra that facilitates desired actions, and an indirect pathway through the globus pallidus that inhibits unwanted actions (Albin et al., 1989; DeLong, 1990; Gerfen et al., 1990; Mink, 2003). There is also a “hyperdirect” pathway through the subthalamic nucleus that rapidly alters basal ganglia output (Nambu et al., 2002). Studies using genetic targeting of striatal neurons in mice have mostly confirmed these functional arrangements and clarified how the direct and indirect pathways work together during the initiation of orienting movements and action sequences (Cui et al., 2013; Jin et al., 2014; Kravitz et al., 2010; Tecuapetla et al., 2016; 2014).

Whether an action should be facilitated or not depends on the expected value of the action given the behavioral context, and there is growing evidence that the functional scope of the basal ganglia includes these more cognitive aspects of action selection. In the primate striatum, the activity of many neurons is related to the value of specific actions, such as making a saccade in a particular direction (Lau and Glimcher, 2008; Lauwereyns et al., 2002a; 2002b) or turning a handle left or right (Samejima et al., 2005). In mice, optogenetic stimulation of striatal neurons can bias orienting choices toward the response port associated with higher rewards (Tai et al., 2012).

The basal ganglia are also implicated in perceptual decision-making tasks (Ding and Gold, 2013), in which action value depends on judging sensory signals, as often happens during natural behavior. In the classic visual motion discrimination task, when the subject decides how to move their eyes based upon the direction of motion in a visual stimulus (Shadlen and Kiani, 2013), neurons in the primate striatum exhibit activity related to several aspects of the decision process (Ding and Gold, 2010), and electrical stimulation of the primate striatum biases perceptual choices as well as the saccades (Ding and Gold, 2012). These results are consistent with clinical findings in humans that basal ganglia dysfunction causes not only motor impairments but also deficits in sensory and cognitive functions (Botha and Carr, 2012; Brown et al., 1997).

The possible involvement of the basal ganglia in perceptual decision- making raises several important questions. Is there a causal link between the activity of striatal neurons and perceptual decision-making? The results from applying electrical stimulation in the primate caudate nucleus provide compelling evidence in favor of a causal role (Ding and Gold, 2012) but leave some key points unresolved. Given the widespread inputs to the striatum from the cortex, including projections from areas known to be involved in decision-making (Haber et al., 2006; Selemon and Goldman-Rakic, 1985), changes in performance with electrical stimulation could be caused by antidromically activating cortical neurons, rather than orthodromically activating circuits through the basal ganglia. Are both the direct and indirect pathways involved? Because electrical stimulation affects neural tissue nonspecifically, it is unclear how the different classes of striatal neurons might have contributed to the stimulation effects.

Can the role of the striatum in perceptual decision-making be dissociated from its role in action selection? In most studies of striatum that involve causal manipulations, the behavior

of the subject involves some form of lateralized movement, such as making a saccadic eye movement or orienting the body. For example, optogenetic stimulation of the mouse striatum has been shown to influence turning to the left or right during locomotion (Kravitz et al., 2010; Tecuapetla et al., 2014), pressing a left or right lever (Cui et al., 2013; Jin et al., 2014), and orienting toward a left or right response port (Tai et al., 2012). These behavioral tasks are well suited to studying action selection, but using the same approach to study perceptual decision-making introduces a potentially serious confound: if stimulation increases rightward choices, is that because sensory decision-making was altered or because the motor output was biased?

Finally, which aspects of decision-making might be regulated by striatal activity? Performance in perceptual tasks can be explained by drift diffusion models in which sensory evidence is accumulated over time until it reaches a decision boundary in favor of a particular choice (Bogacz, 2007; Gold and Shadlen, 2007; Ratcliff and Smith, 2004). However, the possible role of striatal activity in this process remains unclear: does it affect the sensory evidence, the decision boundary, or the motor response? In the primate striatum, some neurons exhibit offsets in their activity that might reduce the amount of evidence needed to reach a decision bound (Ding and Gold, 2010; Lauwereyns et al., 2002b). Other striatal neurons show changes consistent with the accumulation of sensory evidence, but in contrast to neurons in cortical areas (Roitman and Shadlen, 2002), the influence of sensory evidence occurs well before movement onset and does not converge at a fixed value emblematic of a decision boundary (Ding and Gold, 2010). In human fMRI experiments, BOLD signal is elevated in the striatum and frontal cortex when subjects emphasize speed over accuracy, consistent with an effect not on sensory evidence itself, but on the response threshold applied to the evidence (Forstmann et al., 2010; 2008; Ivanoff et al., 2008; van Veen et al., 2008), or relatedly, on the motivation or urgency to make the movement (Mazzoni et al., 2007; Thura and Cisek, 2017).

To address these questions, we used a visual task in mice to investigate the possible causal role of the striatum in perceptual decision-making. Using transgenic mice and optogenetic stimulation, we selectively activated striatal projection neurons in the direct or indirect pathway as mice prepared to detect changes in the orientation of a visual grating. Because the visual changes occurred in either the right or left visual field, and mice always reported their detection by licking a central spout, we were able to identify lateralized changes in perceptual decisions distinct from directional biases in action selection. Our results demonstrate that activation of the direct pathway biases perceptual choices in favor of expected contralateral events, and that these effects are consistent with context-specific changes in response threshold.

Results

We prepared 31 transgenic mice (13 Drd1a-cre and 18 A2a-cre) for targeted optogenetic activation of the striatum with injection of viral vectors (AAV2-EF1a-DIO-hChR2-eYFP or AAV2-EF1a-DIO-eYFP) into the posterior dorsomedial striatum and implantation of a titanium head holder and an optic fiber cannula aimed at the virus injection site (Figure 1A). For brevity, we refer to mice injected with virus containing hChR2 that targeted medium

spiny neurons (MSNs) in the striatal direct and indirect pathway as Drd1a-cre and A2a-cre mice, and the two sets of neurons as dMSNs and iMSNs, respectively; mice injected with virus only containing eYFP are referred to as YFP controls. After recovery from surgery, mice were trained over 6–8 weeks to perform a visual orientation- change detection task.

During the task, head-fixed mice viewed a pair of visual displays, each centered in the left or right visual field, while running on a polystyrene wheel (Figure 1B). Our use of a running wheel, with the visual stimulation linked to locomotor output, is based on previous work demonstrating that this behavioral approach is associated with higher levels of arousal and task engagement (Niell and Stryker, 2010; Poort et al., 2015; Reimer et al., 2014). Based on a randomized distance traveled on the wheel, mice progressed through a sequence of trial epochs (Figure 1C). The typical running speed of the mice in our experiments was 90 cm/s (median: 90.2 cm/s, range across mice: 59.2 to 127.2 cm/s) and each trial lasted several seconds. The sequence of epochs in each trial started with static pink noise on both displays, followed by the addition of a single vertically oriented Gabor patch on either the left or right display; the location of the one patch indicated whether the upcoming stimulus change might occur on the left or right side. A second Gabor patch was then added to the other side, and after a variable distance, the first patch either changed its orientation (change trials) or remained vertical (no-change trials).

The task of the mice was to respond “yes” by contacting a lick spout if an orientation change occurred and to otherwise withhold lick responses. On change trials (50% of total), mice were required to lick within a 500-ms response window after the orientation change to score a “hit” and obtain a liquid reward (Figure 1D); failures to lick or licks after the window were counted as “misses”. On no-change trials (50%), mice should refrain from licking to score a “correct reject”, and licks during the response window were counted as a “false alarms” and resulted in a timeout penalty (Figure 1E). Once mice were proficient in the task, we added trials with optical stimulation. Stimulation was applied on 50% of the trials, randomly interleaved with no-stimulation trials, for a brief interval (50–200 ms after orientation change) chosen to overlap potential MSN visual responses (Reig and Silberberg, 2014) as mice prepared to respond, and to end before the beginning of the lick response window so that it would not directly alter the motor response (Figure 1D–E). Trials with the orientation change on the left or right were run in separate interleaved blocks of 36 trials, and mice typically completed several hundred trials per session (median: 360 trials).

Effects of striatal stimulation on visual detection performance

The effects of stimulating dMSNs are illustrated by data from an example Drd1a-cre mouse for one experimental session that used a single value of orientation change (Figure 1F–I). On change trials (Figure 1F,H), cumulative lick probability increased sharply within the first 200 ms of the response window, indicating that lick responses were time-locked to the orientation changes. Stimulation of dMSNs significantly increased the probability of hit responses, and this increase was larger during contralateral-change blocks (from 78% to 98%, p=0.0011, Chi-square test) than during ipsilateral-change blocks (from 84% to 93%; p=0.10). On no-change trials (Figure 1G,I), stimulation of dMSNs increased the probability of false alarms, and this increase was also larger during contralateral blocks (from 2% to

26%, p<0.001) than during ipsilateral blocks (from 2% to 10%, p=0.06). The increases in hits and false alarms with stimulation points to an added bias in favor of “yes” responses, especially during contralateral blocks.

By varying the amplitude of orientation change, we were able to construct complete psychometric curves and assess how activation of dMSNs changed visual detection performance (Figure 2). For Drd1a-cre mouse #419, histology confirmed transfected neurons in the dorsomedial striatum (Figure 2B) with axonal projections that terminated in substantia nigra pars reticulate (SNr) and other sites consistent with the direct pathway (Figure 2A). This mouse performed 2937 trials across 7 sessions that interleaved 5 values of orientation change, plus no-change trials, to generate the psychometric data and fitted curves plotted in Figure 2C. On trials with no stimulation, lick probability increased from near 0% for orientation changes less than 4° to about 95% for orientation changes greater than 10°, displaying a sensitivity to orientation changes comparable to that reported previously (Glickfeld et al., 2013) and low values for both bias (or guesses) and lapse rate. With stimulation, the psychometric data shifted upwards, with a much larger effect during blocks with contralateral changes than during blocks with ipsilateral changes, demonstrating that the effect of dMSN activation on lick probability depended on the visual field location of the orientation change. Some of the largest changes were observed for orientation changes of 0 degrees (i.e., on no-change trials), indicating that the effect occurred for expected as well as for actual changes in the orientation of the visual stimulus.

We found similar results across the full set of psychometric curves from our sample of Drd1a-cre mice (Figure 2D). Activation of dMSNs caused substantial upward shifts in the psychometric data during contralateral blocks, and only modest shifts during ipsilateral blocks. To quantify these effects, we compared the bias (i.e., the lower asymptote of the fitted function) and the just-noticeable difference in orientation (JND, i.e., the standard deviation of the fitted cumulative Gaussian multiplied by$\sqrt{2}$) observed for trials with and without stimulation. JND is a useful measure of sensitivity, because it indicates the minimum change in orientation that resulted in visual detection at last 50% of the time, independent of response bias and lapse rate. As shown in Figure 2E, stimulation caused a significant increase in bias (contralateral, no stimulation: 0.07 ± 0.05, mean ± 95%CI, with stimulation: 0.45 ± 0.14, p<0.001, paired sample t-test; ipsilateral, no stimulation: 0.05 ± 0.04, with stimulation: 0.19 ± 0.06, p<0.001), and this increase was significantly larger for contralateral than for ipsilateral (p = 0.0013, two-way ANOVA). In contrast, as shown in Figure 2F, stimulation had non-significant effects on JND (contralateral, no stimulation: 4.18 ± 0.90°, with stimulation: 3.52 ± 1.00°, p=0.16, paired sample t-test; ipsilateral, no stimulation: 3.89 ± 0.96°, with stimulation: 3.24 ± 0.76°, p=0.26) that were not different between contralateral and ipsilateral blocks (p = 0.98, two-way ANOVA).

Activation of iMSNs also produced changes in bias but these effects did not depend on the location of the expected visual event (Figure 3). The example A2a-cre mouse #403 contained transfected neurons in the dorsomedial striatum (Figure 3B) with projections that terminated in the external segment of the globus pallidus (GPe), as expected for iMSNs (Figure 3A). This mouse performed 2908 trials across 8 sessions to generate psychometric data that again exhibit an orderly relationship between lick probability and the size of the

orientation change (Figure 3C). Stimulation of iMSNs shifted the psychometric data upwards, and the size of this shift did not depend on whether the visual event was expected contralateral or ipsilateral; similar results were found across our sample of A2a-cre mice (Figure 3D). Quantifying these effects, as shown in Figure 3E, we found that stimulation caused a significant increase in bias (contralateral, no stimulation: 0.06 ± 0.03, with stimulation: 0.34 ± 0.09, $p<0.001$; ipsilateral, no stimulation: 0.05 ± 0.02, with stimulation: 0.37 ± 0.10, $p<0.001$) but there was no difference between the effects elicited during contralateral and ipsilateral blocks ($p = 0.53$). Stimulation had variable effects on JND (Figure 3F, contralateral, no stimulation: 3.61 ± 0.67°, with stimulation: 4.10 ± 1.65°, $p=0.54$; ipsilateral, no stimulation: 2.85 ± 0.64°, with stimulation: 3.67 ± 0.99°, $p = 0.11$) that were not significant and that did not differ between contralateral and ipsilateral blocks ($p = 0.74$).

To confirm that these effects on psychometric performance were due to manipulation of dMSNs and iMSNs, and not the consequence of some nonspecific effect of optical stimulation, we conducted the same experiments in a set of YFP control mice (n=8). These mice generated psychometric data comparable to that from the Drd1a-cre and A2a-cre mice described above, except that stimulation caused no changes in performance (Figure 4A). Analysis of the bias (Figure 4B, contralateral, no stimulation: 0.05 ± 0.03, with stimulation: 0.07 ± 0.03, $p = 0.06$; ipsilateral, no stimulation: 0.07 ± 0.03, with stimulation: 0.05 ± 0.03, $p = 0.12$) and JND (Figure 4C, contralateral, no stimulation: 4.24 ± 0.80°, with stimulation: 3.67 ±1.44°, $p = 0.31$; ipsilateral, no stimulation: 3.95 ± 0.68°, with stimulation: 3.68 ± 1.07°, $p = 0.60$) from these mice verified that there was no spatial effect of stimulation (bias: $p = 0.20$; JND: $p = 0.75$).

To directly compare the effects of dMSN and iMSN activation, we tabulated the changes in response bias and JND for each set of mice. This comparison illustrates that the main effect was an increase in response bias (Figure 5A), with no significant effects on JND (Figure 5B). For dMSNs but not iMSNs, stimulation caused larger changes in bias when the visual event was expected in the contralateral visual field. These effects are also evident by comparing the population psychometric curves obtained by pooling data across all Drd1a or A2a mice. Activation of dMSNs caused a larger upward shift of the performance curve (Figure 5C) during contralateral (orange) than ipsilateral (blue) blocks, whereas activation of iMSNs shifted both curves equally (Figure 5D). The effects on response bias but not JND indicate that activation of MSNs did not change the quality of the sensory evidence, but instead revealed a visual-field asymmetry in the commitment to response “yes”.

In addition to these change in performance accuracy, activation of dMSNs and iMSNs also affected response latency. For analyzing latency, because there were many fewer responses to small orientation changes, we pooled data across mice to improve the power of the statistical analysis. Activation of dMSNs tended to decrease response latency, and consistent with the effects on psychometric curves, this effect was observed when visual events were expected in the contralateral (Figure 5E) but not the ipsilateral (Figure 5G) visual field. Activation of iMSNs had more complex effects on response latency that depended on whether the orientation change was likely to be detected. For orientation changes detected less than half the time, iMSN stimulation decreased response latency, regardless of whether

the event occurred in the contralateral (Figure 5F) or ipsilateral (Figure 5H) visual field. However, for orientation changes detected more than half the time, iMSN stimulation increased response latency, but only for visual events expected in the contralateral visual field. Together, these results indicate that activation of dMSNs and iMSNs had opposite effects on the speed of responding to easily detected visual events, but only for changes or expected changes in the contralateral visual field.

Finally, these effects on choice behavior were not related to changes in movement vigor during the detection task. Optogenetic stimulation did not change the strength of the lick responses, or the overall number or frequency of licks (Figure S2). Activation of either dMSNs or iMSNs had a tendency to transiently decrease running speed, but with no asymmetry based on contralateral or ipsilateral blocking of trials (Figure S3). Running speed had an influence on overall psychometric performance, but no effect on response bias, the parameter affected by MSN activation (Figure S4), and regardless of running speed, MSN activation altered detection performance by changing response bias, but not sensitivity (Figure S5). Thus, we did not find evidence that activation of dMSNs increased the vigor of the motor output; instead, our evidence supports the interpretation that activation altered the strength of the commitment to respond.

Time course of the striatal effect on response criterion and latency

The lateralized effects found with stimulation of dMSNs and iMSNs indicate that the mice applied a different bias in each block based on the expected location of the rewarded visual event, and this affected both response accuracy and speed. To explore the time course of these effects, we examined how the effects of stimulation varied across the 36 trials that comprised each block. For this analysis, we used a single supra-threshold value (12°) of orientation change, pooled the results across mice to achieve reasonable statistical power, and assigned each trial outcome to a bin corresponding to its trial number within the 36-trial block. We then tabulated hits and false alarms, and computed response criterion for each trial number within a block, using standard signal detection theory (Macmillan and Creelman, 2005), as well as response latency, separately for trials with and without stimulation, and for contralateral and ipsilateral blocks. Finally, we plotted the changes in response criterion and response latency caused by stimulation (Figure 6).

For response criterion, this analysis revealed that it took about 5 trials on average for a significant visual field asymmetry to emerge in the effects of dMSN stimulation (asterisks in Figure 6A), and this asymmetric effect on bias remained fairly constant for the rest of the block. Stimulation of iMSNs (Figure 6B) caused a smaller change in response criterion with a possible delayed asymmetry in favor of the ipsilateral visual field that did not reach significance. The time course of these effects indicates that it takes only a handful of trials for the expectation about the location of the visual event to develop within each block.

For response latency, we found that with dMSN stimulation it took about 12 trials on average for a significant decrease in the response latency for contralateral visual events to emerge (filled orange symbols below zero in Figure 6C), but there was no consistent change in latency for ipsilateral visual changes (blue symbols in Figure 6C). Stimulation of iMSNs caused the complementary effect: it took about 9 trials for a significant increase in response

latency for contralateral visual events to emerge (filled orange symbols above zero in Figure 6D), with a slight decrease in latency for ipsilateral visual events that did not consistently reach significance (blue symbols in Figure 6D). These results confirm that activation of dMSNs and iMSNs had opposite effects on the response latency specifically for visual events in the contralateral visual field.

Dependence on the presence of choice-relevant visual stimuli

In the results presented above, because we were interested in visual detection performance, the stimulation of the dMSNs and iMSNs was applied shortly after the Gabor patch orientation change. However, because stimulation increased lick probability even in the absence of an orientation change, this raises the possibility that similar results might be found regardless of when the stimulation was applied, and might be due to a nonspecific increase in the tendency to lick. To test this possibility, we ran a control experiment in the same mice in which we systematically varied when the stimulation was applied during the sequence of trial epochs.

This control experiment was predominated by normal trials (40/55 trials per block) with the same structure as the original visual detection task outlined in Figure 1, with stimulation on 50% of these trials. To simplify the interpretation, we focused on the no-change trials and first replicated our finding that stimulation increased lick probability when applied while the mice viewed the two Gabor patches (Figure 7, first two columns). Consistent with our previous results, in the original two-patch condition (2nd column) stimulation of dMSNs produced a larger increase ($p < 0.001$) in lick probability when the change was expected in the contralateral visual field (Figure 7B, contralateral, no stimulation: 0.05 ± 0.03, with stimulation: 0.47 ± 0.12, $p < 0.001$; ipsilateral, no stimulation: 0.05 ± 0.02, with stimulation: 0.19 ± 0.07, $p < 0.001$), and stimulation of iMSNs increased lick probability equally ($p = 0.68$) for both sides (Figure 7C, contralateral, no stimulation: 0.05 ± 0.02, with stimulation: 0.26 ± 0.05, $p < 0.001$; ipsilateral, no stimulation: 0.06 ± 0.03, with stimulation: 0.28 ± 0.05, $p < 0.001$). Interleaved with these original conditions, we included what we called “sequence-arrested control trials” (three trial types, each has 5/55 trials per block). These control trials began like normal trials, but rather than progressing through the full sequence of visual epochs, the sequence was stopped once the visual display reached a particular benchmark – specifically, one Gabor patch or visual noise or just the blank gray background (Figure 7A). On these control trials the mice continued to run on the wheel, and the stimulation was applied as before at a particular randomized distance, but with the mice viewing a reduced version of the normal visual content.

If stimulation of striatal MSNs caused a nonspecific increase in lick probability – for example, by adding a motor signal that promoted licking – then it should not matter what the mice were viewing when the stimulation was applied. To the contrary, we found that the effects of striatal stimulation depended on the content of the visual display. When stimulation was applied while mice viewed one Gabor patch (Figure 7, 3rd column, Drd1a-cre, contralateral: 0.24 ± 0.10, ipsilateral: 0.08 ± 0.03; A2a-cre, contralateral: 0.15 ± 0.06, ipsilateral: 0.14 ± 0.05) the effect on lick probability was about half as large as in the normal two-patch condition. When stimulation was applied while mice viewed either visual noise

(Drd1a-cre, contralateral: 0.03 ± 0.03, ipsilateral: 0.01 ± 0.01; A2a-cre, contralateral: 0.02 ± 0.02, ipsilateral: 0.02 ± 0.02) or just the gray background (Drd1a-cre, contralateral: 0.02 ± 0.02, ipsilateral: 0.01 ± 0.01; A2a-cre, contralateral: 0.03 ± 0.02, ipsilateral: 0.02 ± 0.02), the effect went away entirely (Figure 7, right columns). These results demonstrate that the effect of striatal stimulation was not a generalized increase in response probability, but was specific to task epochs in which choice-relevant visual stimuli were present.

Detection-related activity of medium spiny neurons in the direct pathway

To identify the neuronal signals present in the dorsomedial striatum during the visual detection task, we prepared an additional 8 mice for fiber photometry, a method for measuring intracellular Ca^{2+} fluctuations from a population of neurons (Cui et al., 2013; Lerner et al., 2015) We expressed GCaMP6f in dMSNs by injection of viral vectors (AAV5-DIO-GCaMP6f) into the dorsomedial striatum of Drd1a-cre mice and implantation of an optic fiber for delivering excitation light and recording the emitted GCaMP6f signal (Figure 8A).

The most consistent signal we observed was a phasic lick-related increase (Figure 8B). The onset of this activity occurred 160.8 ms before lick onset (contralateral: 172.0 ± 25.6ms; ipsilateral: 149.7 ± 35.7ms, p = 0.71, paired non-parametric Wilcoxon test) and peaked 198.6 ms after the onset of the first lick (contralateral: 197.6 ± 50.6ms, ipsilateral: 199.7 ± 43.2ms, p = 0.93). When aligned on the time of the orientation change, the onset occurred 226.1 ms after the visual stimulus change (contralateral: 224.1 ± 11.7ms, ipsilateral: 228.1 ± 12.2ms, p = 0.78, Figure S6). The timing of this phasic activity indicates a role in the decision to lick, but does not clearly distinguish between feedforward control of licking or feedback about the impending decision. A more definitive finding was that this phasic activity was not associated with all licks during the task, but only to those licks that were related to detecting the change in the visual stimulus. As shown by the population averages aligned on lick onset (Figure 8C), this phasic GCaMP6f signal was observed for lick responses made while the mice viewed the two Gabor patches, whether these licks were hits (Figure 8C, change) or false alarms (“change”). Similarly, licks made earlier during the two-patch trial epoch, at running distances that fell short of the normal range of orientation-change events, were also associated with phasic increases in signal (Figure 8C, two patch). In contrast, phasic increases were less apparent for licks that occurred during the one-patch epoch, and were completely absent for licks that occurred during the earlier epochs when only noise or gray background were visible.

To quantify and compare these results, we measured the lick-related changes in GCaMP6f for each of these trial epochs in each mouse. Confirming the pattern shown by the population average traces, there were significant changes in normalized ΔF/F transients for licks that occurred while mice viewed the two Gabor patches (Figure 8D, three left plots, change, contralateral: 0.51 ± 0.30%, p = 0.007, t-test, ipsilateral: 0.48 ± 0.42%, p = 0.037; ‘change’, contralateral: 0.44 ± 0.25%, p = 0.004, ipsilateral: 0.43 ± 0.25%, p = 0.005; two patch, contralateral: 0.44 ± 0.32%, p = 0.015, ipsilateral: 0.33 ± 0.28%, p = 0.027) but not for licks that occurred during one patch or the noise-grey background (Figure 8D, right two plots, one patch, contralateral: −0.02 ± 0.35%, p = 0.89, t-test, ipsilateral: 0.18 ± 0.38%, p =

0.30; noise-grey, contralateral: −0.02 ± 0.14%, p = 0.76, ipsilateral: −0.14 ± 0.25%, p = 0.22). This dependence on trial epoch indicates that the lick-related modulation of dMSNs was specific to reporting the perceived change in the visual stimulus, rather than a general motor signal related to licking. Moreover, the GCaMP6f signal did not show a difference between visual events expected in the contralateral versus the ipsilateral visual field, unlike the lateralized effects found with stimulation. This suggests that the asymmetric effect of stimulating dMSNs is due to circuits that are downstream from the striatum.

Discussion

Our results demonstrate a causal link between neuronal activity in the striatum and visual decision-making in mice. Using optogenetic stimulation in transgenic mice trained to perform a visual orientation-change detection task, we found that activation of MSNs in the striatum induces a perceptual decision bias – a lateralized change in response threshold to visual events. We were able to identify effects on perceptual decision-making, distinct from changes in motor control, because the optogenetic stimulation and visual events during the task were lateralized, whereas the behavioral choice (lick or don't lick) was not. This approach revealed that the behavioral effects of activating striatal neurons depend on the visual context. First, for the direct pathway, the stimulation-induced effects on performance accuracy were significantly larger when the visual event was expected in the contralateral visual field. Second, stimulating the direct and indirect pathways had opposite effects on response latency that were specific to visual events in the contralateral visual field – activation of dMSNs decreased latency and activation of iMSNs increased latency. Third, for both direct and indirect pathways, the effects were observed only during task epochs in which the choice-relevant visual stimuli were present. Finally, the choice-related GCaMP activity we recorded during the task was also specific to responses made in the presence of task-relevant visual stimuli. Thus, in addition to demonstrating a causal role of the striatum in perceptual decision-making, our results show that striatal activation biases decisions in favor of expected or valued visual events.

The striatum and perceptual decision-making

Previous studies have provided evidence that activity in the striatum might be related to regulating the response threshold applied during decision-making or perhaps to evidence accumulation itself, although the tasks in these studies were not specifically designed to distinguish between changes in perceptual decision- making versus biases in motor preparation. In the monkey, neuronal recordings from caudate nucleus during a saccade task found higher activity when the contralateral target was associated with a higher reward, and this bias was present even before the visual stimulus was presented (Lauwereyns et al., 2002b). Similarly, during a visual motion discrimination task, caudate neurons exhibit activity related to choice bias, as well as to the accumulation of sensory evidence and the strength of the motion signal (Ding and Gold, 2010). Electrical microstimulation of the monkey caudate nucleus induced a choice bias during the motion discrimination task, and this bias was well explained with a drift diffusion model by changing the starting value of the decision variable (Ding and Gold, 2012). In human functional imaging studies, more rapid decisions were associated with increases in BOLD activity in the striatum, as well as in

frontal, prefrontal and parietal cortical areas (Forstmann et al., 2008; Ivanoff et al., 2008; van Veen et al., 2008), and the ability of subjects to control the tradeoff between speed and accuracy was associated with stronger connections between the cortex and striatum (Forstmann et al., 2010). Together, these studies indicate a role for the basal ganglia in regulating the readiness to make the choice.

Computational models reinforce this view of how the basal ganglia contribute to performance during perceptual decision tasks. In a network model that explains performance in visual motion discrimination task (Lo and Wang, 2006), the model equivalent of the direct pathway through the basal ganglia adjusts the threshold level of evidence that is required to trigger the saccade response, whereas the accumulation of sensory evidence is assumed to take place in the cerebral cortex. Another model of perceptual decision-making makes the point that, in order to perform optimally, the value of the decision variable for the presumptive choice should be adjusted based on the strength of the competing alternatives, and that the properties of the basal ganglia make it especially well-suited to carry out this function (Bogacz and Gurney, 2007).

Our experiments provide direct causal evidence that circuits through the striatum contribute a context-specific bias during perceptual decision tasks. We found that activation of the striatum shifted the psychometric curves upward and altered reaction times, consistent with a change in the response threshold or the strength of the commitment to respond (Thura and Cisek, 2017; Turner and Desmurget, 2010). We found no change in the sensitivity of visual detection, indicating that striatal activation did not directly affect the quality of sensory processing or how the sensory evidence was accumulated. On the other hand, activation of the striatum did not increase the probability of licking or alter the vigor of licking movements (Figure S2). Instead, we found that striatal stimulation regulated the readiness to lick only in very specific circumstances: when behaviorally relevant visual stimuli were present and when the visual event was expected in the contralateral visual hemifield. The measurements of striatal activity provided by GCaMP signals confirm the dependence on visual context – we found striatal activity before and during the lick response, but only for licks evoked in the presence of behaviorally relevant visual stimuli. Our results therefore demonstrate that circuits through the basal ganglia can bias perceptual choices by changing the response threshold for a specific sensory-guided action in the appropriate behavioral contexts.

Implications for circuits through the basal ganglia

The direct pathway through the basal ganglia is associated with facilitating desired actions through disinhibition. It originates with medium spiny neurons in the striatum that project directly to basal ganglia output nuclei such as the substantia nigra, and because both the striatal and output projections are inhibitory, an increase in the activity of direct pathway striatal neurons reduces the tonic inhibition exerted by output nuclei on their targets (Gerfen and Surmeier, 2011; Mink, 2003). Perhaps the best known example is how striatal modulation of the substantia nigra gates the orienting movements controlled by the superior colliculus (Hikosaka et al., 2000). In monkeys, disinhibition of the superior colliculus on one side of the brain evokes saccades directed into the contralateral visual field (Hikosaka and

Wurtz, 1985a; 1985b). Similarly, in rodents, nigra-projecting striatal neurons increase their activity during body turns toward the contralateral side (Cui et al., 2013; Tecuapetla et al., 2014), and optogenetic activation of these neurons induces contraversive turning behavior (Kravitz et al., 2010).

Our results extend this picture by highlighting the importance of sensory- motor topography even for perceptual choices that do not involve lateralized movements. As expected from disinhibition of movement-related circuits, we found that activation of the direct pathway increased the probability of lick responses and decreased reaction times. However, because the licks always involved the same central spout, the lateralized effects we found cannot be attributed to the organization of the motor output, but instead reflect the organization of the inputs and outputs of the basal ganglia. The cortical inputs to the striatum are predominantly uncrossed and represent the contralateral sensory fields, with weaker inputs from ipsilateral sensory fields (Reig and Silberberg, 2016; 2014), in keeping with the larger effects we found for contralateral visual conditions. The dorsomedial part of the striatum, which we targeted, receives inputs from visual cortex and frontal association areas (Hintiryan et al., 2016), consistent with our finding of effects for expected (i.e., on no-change trials) as well as actual visual events. The outputs of the basal ganglia have a complex organization, but the lateralized visual effects we found by activating MSNs indicates that the circuits through the basal ganglia preserve at least some elements of this visual specificity. For example, one simple possibility is that the sensory-motor structures targeted by the basal ganglia activation in our experiments also receive predominantly uncrossed cortical inputs (Figure S1); activation of dMSNs would thus tend to facilitate licks that were evoked mostly by stimulus events expected in the contralateral visual field.

Our results also illustrate that these sensory-motor circuits get facilitated only in very particular behavioral contexts – in our case, defined by the presence of particular visual stimuli. The changes in perceptual choice behavior that we observed by stimulating MSNs presumably reveal the mappings between visual context and action values that our mice learned during training (Sutton and Barto, 1998); these mappings could be implemented by tailoring the pattern of basal ganglia inhibition to the current visual context (Figure S1). Because the features of the environment constantly change, both in our task and elsewhere, we propose that correctly recognizing the visual context is often a major limiting factor in identifying the desired action. This interpretation is consistent with findings that value coding in the monkey striatum has been found not just for actions (Lauwereyns et al., 2002b; Samejima et al., 2005), but also for visual objects (Kim and Hikosaka, 2013; Yamamoto et al., 2012). It also suggests the intriguing possibility that activation of the striatum causes contralateral turning, not just because downstream orienting circuits are recruited, but also because activation simulates the presence of valued objects in the contralateral side of the visual field.

In contrast to the direct pathway, the indirect pathway is associated with inhibiting unwanted actions, and includes projections through additional nuclei before influencing the output of the basal ganglia (Gerfen and Surmeier, 2011; Mink, 2003). Classic models of basal ganglia function originally proposed that the function of the indirect pathway in action selection was opposite to that of the direct pathway (Albin et al., 1989; DeLong, 1990). More recent

studies have clarified that activity in both pathways contributes to turning behavior in mice (Kravitz et al., 2010; Tecuapetla et al., 2014), the initiation of action sequences (Cui et al., 2013; Tecuapetla et al., 2016), and performance during choice tasks (Tai et al., 2012); the net effect on the motor output depends on the relative amplitude and timing of activity in the direct and indirect pathways.

Some of our results are consistent with antagonistic roles for the direct and indirect pathways during perceptual decision-making. For contralateral visual orientation changes that exceeded the perceptual threshold, we found that activation of iMSNs increased reaction times and activation of dMSNs decreased reaction times (Figures 5,6). Thus, activity in the direct pathway promoted the action linked to the contralateral event, whereas activity in the indirect pathway inhibited, or at least delayed, that action. A recent study in the monkey also shows that the indirect pathway conveys signals that help suppress movements toward visual objects that are not valued (Kim et al., 2017).

However, some of our other results do not fit neatly within this dichotomy. For visual orientation changes below threshold, we found that activation of either iMSNs or dMSNs decreased reaction times and increased the probability of licks. It is not clear why activation of the direct and indirect pathways produced similar outcomes in the absence of a detectable visual event. One possibility is that our measurement of licks is too simple to detect the relevant variable, since it does not capture the full complexity of licking behavior (Vrtunski and Wolin, 1974; Weijnen, 1998). Another possibility is that the functions of the two pathways converge under some conditions, perhaps mediated by projections to shared targets including the GPe (Wu et al., 2000). It is also possible that the evoked effects depend on the detailed timing and patterning of MSN activation. Most previous striatal activation experiments used much longer durations of light stimulation that overlapped or abutted action initiation (Kravitz et al., 2010; Tai et al., 2012; Tecuapetla et al., 2016). In our experiments, activation of iMSNs was brief (150 ms) and ended before the first possible lick; if iMSN stimulation were applied during the time of actual licking, the results might be different. Neuronal recordings from iMSNs in our task, which are missing from this study, would help clarify how these stimulation patterns compare to the normal time course of activity.

Other results point more clearly to complementary but not necessarily antagonistic roles for the direct and indirect pathways during perceptual decision-making. Specifically, we found that the effects of dMSN activation on response rate depended on the location of the expected visual event, but the effects of iMSN activation did not. This difference may have an anatomical basis, because there is evidence that sensory and limbic structures preferentially target dMSNs rather than iMSNs (Wall et al., 2013), and dMSNs show a preference for contralateral visual stimulation, whereas iMSNs do not (Reig and Silberberg, 2014; Sippy et al., 2015). This difference is also consistent with the complementary roles proposed for the direct and indirect pathway in some models of the basal ganglia. In a model of perceptual decision-making (Bogacz and Gurney, 2007), activity in the direct pathway is presumed to be proportional to the sensory evidence for a particular action, and thus might be expected to depend on particular visual inputs; in contrast, activity in the indirect pathway represents the salience of all the other options, and thus might involve pooling signals across

the visual field. A similar distinction was made in an earlier model of action selection (Gurney et al., 2001). Our current experiments do not specifically test these ideas about how the direct and indirect pathways might interact, because we did not include multiple options or irrelevant visual events. Investigating these task variations, as well as targeting other components of the circuit and varying the timing of the manipulations, is likely to provide additional important insights into how the basal ganglia contribute to perceptual decision-making.

STAR Methods

CONTACT FOR REAGENT AND RESOURCE SHARING

Further information and requests for resources should be directed to and will be fulfilled by the Lead Contact: Richard J. Krauzlis (Richard.krauzlis@nih.gov)

EXPERIMENTAL MODEL AND SUBJECT DETAILS

Animals—Procedures were conducted on a total of 49 mice from two BAC-mediated transgenic lines from GENSAT (Gerfen et al., 2013): Drd1a-Cre, (B6.FVB(Cg)-Tg(Drd1a-cre)EY217Gsat/Mmucd; MMRRC #034258-UCD), mice with Cre-recombinase expressed in striatonigral neurons (n=27), and A2a-Cre, (B6.FVB(Cg)-Tg(Adora2a-cre)KG139Gsat/Mmucd; MMRRC #036158-UCD), mice with Cre-recombinase expressed in striatopallidal neurons (n=22). Results reported in the paper are based on data from 39 mice; 10 of the 49 total mice were excluded from the study either because of premature implant failure or inability to learn the task within three months of training. Mice from both transgenic lines had been backcrossed with C57BL/6J (Jackson Laboratory, Bar Harbor, ME) for at least two generations after establishment of the colonies. Mice were derived from heterozygotes mated with wild-type C57BL/6J mice, producing heterozygotes and wild-type littermates. All the animals used in the study were heterozygotes. Among the 39 mice used in the paper, 32 were male and 7 were females. We did not observe any systematic difference in behavioral performance between genders in this study. The mice were housed in a 12:12 reversed day-night cycle, with lights off at 9 am, and all experimental procedures and behavioral training were done in the lights-off portion of the cycle (9am-9pm). Male and female mice weighing 18–25 grams were surgically implanted at age 6–8 weeks and then used in experiments for up to ~9 months. All the mice were in group housing (2–4 cage mates) prior to the surgical procedure, and subsequently singly housed after the implant surgery. All experimental procedures and animal husbandry were approved by the NIH Institutional Animal Care and Use Committee (IACUC) and complied with Public Health Service policy on the humane care and use of laboratory animals.

Viral vectors—Adeno-associated viral vectors (AAVs) were used to express one of three possible products: channelrhodopsin, yellow fluorescent protein (YFP), or GCaMP6f. Double-floxed inverted (DIO) recombinant AAV vector (AAV2) was used to express light-gated channel channelrhodopsin (hChR2(H134R)-eYFP), or the enhanced yellow fluorescent protein (eYFP) in Cre-expressing neurons in the dorsomedial striatum. The double-floxed reverse hChR2-eYFP cassette was driven with a EF-1a promoter and WPRE to enhance expression. The recombinant AAV vector was serotyped with AAV2 coat

proteins and packaged by the University of North Carolina viral core (titer of $4x10^{12}$ particles/ml). Another flip-excision (FLEX) recombinant AAV5 was used for Cre-dependent expression of fast calcium indicator GCaMP6f (AAV5-hSyn-FLEX-GCaMP6f-WPRE-SV40), packaged by the University of Pennsylvania School of Medicine Viral Core (titer of $4x10^{12}$ particles/ml).

METHOD DETAILS

Stereotaxic surgery—Each mouse was injected with virus unilaterally and implanted with a head-holder and optic fiber during a single surgical procedure. During the surgery, animals were anesthetized with isoflurane (4% induction, 0.8–1.5% maintenance) and secured by a stereotaxic frame with ear bars (Kopf Instruments). Dexamethasone (1.6 mg/kg) was administered to reduce inflammation. A feedback-controlled heating pad (FHC) was used to maintain the body temperature at 37°C, and artificial tears were appl ied to the eyes to prevent them from drying. After animal's head was leveled with the stereotaxic frame, a scalp incision was made along the midline, followed by a small craniotomy for virus injection and optic fiber implantation. The coordinates for the unilateral virus injection were ±1.8~2.5mm from midline (M-L axis), 0~0.5mm from Bregma (A-P axis) and 2.5–3mm ventral (D-V axis), based on a standard mouse brain atlas (Paxinos and Franklin, 2004). Each mouse was injected with 0.2–0.3 microliter of virus at a flow rate of 50 nl/min, using a manual microinjector (Sutter Instrument) with 30μm-tip pulled glass pipettes. For the Drd1a-Cre mice included in the results, 11 were injected with DIO-ChR2-eYFP virus, 2 were injected with DIO-eYFP virus, and 8 were injected with FLEX-GCaMP6f virus. For A2a-Cre mice, 12 were injected with DIO-ChR2-eYFP virus, and 6 were injected with DIO-eYFP. An optic fiber (200μm core) together with its ceramic ferrule base (Plexon Inc.) were subsequently inserted at the injection coordinates with the fiber tip located at 0.3~0.5mm above the injection center. A custom-designed titanium head post for head-fixing was positioned and secured to the skull together with the ferrule using Metabond (Parkell Inc.). The skin wound edge was then closed with sutures or tissue adhesive (3M Vetbond). After surgery, mice received subcutaneous ketoprofen (1.85mg/kg) daily for up to three days to ease discomfort. Functional expression of ChR2 was confirmed several weeks after the surgery by open field behavioral analysis (Kravitz et al., 2010), which tested whether blue light delivered through the implanted fiber could induce turning behavior. Fiber placement and viral expression were validated histologically in all mice after completion of data collection.

Food control—After mice recovered from surgery and returned to above 95% of their pre-surgery weight (typically within 7–9 days), they were placed on a food control schedule. Mice had free access to water, but their intake of dry food was controlled, and they were allowed to augment their dietary intake by access to a nutritionally complete 8% soy-based infant formula (Similac, Abbott, IL). Overall food intake was regulated to maintain at least 85% of their free-feeding body weight, and the health status of each mice was monitored daily throughout the study. Mice were initially acclimatized to handling procedures by having their heads gently restrained while receiving the soy-based fluid under manual control via a sipper tube. After the initial exposure to soy-based fluid, we more securely head-fixed the animal and continued manual delivery. Once mice were adapted to these

procedures, we switched to automatic delivery of fluid under computer control in the behavioral apparatus.

Behavioral apparatus—The behavioral apparatus consisted of a custom-built booth that displayed visual stimuli to the mouse coupled to their locomotion. The mouse was head-fixed in the center of the apparatus, positioned atop a polystyrene foam wheel (20-cm diameter) that allowed natural walking or running movements along a linear path. An optical encoder (Kübler) was used to measure the rotation of the wheel. The front walls of the booth incorporated a pair of LCD displays (ViewSonic VG2439) positioned at 45° angles from the animal's midline such that each display was centered on either the right or left eye and subtended ~90° horizontal by ~55° vertical of the visual hemifield, with a viewing distance of 27.5 cm. The interior of the booth was lined with sound absorbent material to reduce acoustic noise. The experiments were controlled by a computer using a modified version of the PLDAPS system (Eastman and Huk, 2012). Our system omitted the Plexon device, but included a Datapixx peripheral (Vpixx Technologies, Saint-Bruno, QC, Canada) and the Psychophysics Toolbox extensions (Brainard, 1997; Pelli, 1997) for Matlab (The Mathworks, Natick, MA, USA), controlled by Matlab-based routines run on a Mac Pro (Apple, Cupertino, CA, USA). The Datapixx device provided autonomously timed control over analog and digital inputs and outputs, and synchronized the display of visual stimuli generated using the Psychophysics Toolbox. A reward delivery spout was positioned near the snout of the mouse; lick contacts with the spout were detected by a piezo sensor (Mide Technology Co., Medford, MA, USA) and custom electronics. Each reward was a small volume (5–10 μl) of an 8% solution of soy-based infant formula (Similac, Abbott, IL) delivered by a peristaltic pump (Harvard Apparatus) under computer and Datapixx control. Airpuff aversive stimuli were delivered through a second spout located slightly above the reward spout, and controlled through solenoids (Parker Hannifin, Cleveland, OH, USA). The temperature inside the apparatus maintained between 70–80° F.

Visual detection tasks—Animals were run in experiments on alternating days and each session produced 300–800 trials. Experiments were organized in blocks of randomly shuffled, interleaved trials, and each trial consisted of a sequence of epochs that the mouse passed through by walking or running on the wheel. Each epoch was defined by the particular stimuli presented on the visual displays, and the duration of each epoch was determined by the time that it took for the mouse to travel a randomized distance on the wheel, typically several seconds based on the running speed of the mice (median: 90.2 cm/s).

In all of the experiments, with the exception of the "sequence arrested" control experiments described below, each trial followed a standard sequence of four epochs. The average luminance across each visual display in all epochs was 4–8 cd/m^2. In the first epoch ("noise"), the uniform gray of the inter-trial interval was changed to pink visual noise with an RMS contrast of 3.3%; this epoch was presented for a distance of 0.9–1.8 cm (i.e., 0.007–0.03 s). In the second epoch ("one patch"), a vertically oriented Gabor patch was added to the pink noise, centered in either the left or right visual display. The Gabor patch consisted of a sinusoidal grating (95% Michelson contrast) with a spatial frequency of 0.1 cycles per

degree, a value chosen based on the visual spatial acuity of mice (Prusky et al., 2004; Schmucker et al., 2005; Sinex et al., 1979), modulated by a Gaussian envelope with full width at half-maximum of 18° (σ = 7.5°). The phase of the grating was not fixed, but throughout the trial was incremented in proportion to the wheel rotation with every monitor refresh, so that the sinusoidal pattern was displaced on the screen by approximately the same distance that the mouse traveled on the wheel; the Gabor patch on the left (right) drifted leftward (rightward), consistent with optic flow during locomotion. This second epoch lasted for 46–92 cm (0.36–1.55 s). In the third epoch ("two patches"), a second Gabor patch with the same properties appeared on the other side of the visual display, and this epoch lasted for 107–214 cm (0.84–3.6 s). The visual stimuli in the fourth epoch depended on whether the trial was a "change" or "no change" condition; the two types were equally likely and randomly interleaved within a block, and both lasted 77–154 cm (0.61–2.6 s). On change trials, the Gabor patch that had appeared first, during the one-patch epoch, changed its orientation at the onset of the fourth epoch. The direction of the orientation change observed mirror symmetry: if the left (right) Gabor changed, it rotated clockwise (counterclockwise). On no-change trials, the two Gabor patches did not change their orientation, so that the fourth epoch unfolded as a seamless extension of the previous two-patch epoch.

The task of the mouse was to lick the spout when he or she detected a change in the orientation of the Gabor patch and to otherwise withhold from licking. Mice were required to lick within a 500-ms response window starting 300 ms after the orientation change in order to score a "hit" and receive a fluid reward. If the mouse failed to lick within this window after an orientation change, the trial was scored as a "miss" and no reward was given but no other penalty was applied. On no-change trials, if the mouse licked within the same response window aligned on the transition to epoch 4, the trial was scored as a "false alarm"; if they correctly withheld from licking, the trial was scored as a "correct reject". At the end of correct reject trials, the trial was extended to include an additional "safety-net epoch" in which the initially appearing Gabor underwent a supra-threshold (30°) orientation change and the mouse could receive a reward by licking within a comparable response window. The point of this safety-net epoch was to maintain motivation by rewarding the mouse for correct behavior without violating the task rule that they should lick only for orientation changes. False alarms and premature licks before the response window led to timeouts and possible air-puff penalties; well-trained mice usually committed fewer than 10% of such errors.

In three sets of experiments (psychometric curves, time course, and fiber photometry), all trials followed the standard 4-epoch trial sequence and were organized into alternating blocks in which the orientation change occurred in either the left or right Gabor patch. We counterbalanced the frequency of trials with and without orientation changes, and with and without stimulation, in order to minimize possible behavioral biases related to frequency matching.

For the psychometric curve experiments, we used a block length of 40 trials: 25% with change and no stimulation, 25% with no change and stimulation (described below), 25% with an orientation change drawn equally from five possible values (4, 7, 11, 15, 20°) and with no stimulation, and 25% with the same five orientation changes with stimulation.

Because only some of the orientation changes could be reliably detected, a safety-net epoch was added to the end of miss trials, but with a long duration to discourage using it as a default response. We recorded 7–9 sessions for each mouse to obtain at least 60 repetitions for each of the five orientation changes.

For the time course and fiber photometry experiments, we used a block length of 36 trials and a single value of 12° for the orientation change. For the time course experiments, each of the 4 possible combinations of two factors (change/no-change, stimulation/no stimulation) comprised 25% of the total trials in each block. For the fiber photometry experiments, change and no-change trials were equally likely (50% in each block), and the durations of the pre-trial gray screen and the noise epoch were lengthened, in order to provide longer baselines for measuring the GCaMP signal. We recorded 10–12 sessions in these experiments for each mouse to obtain at least 250 repetitions for each trial type.

In the "sequence arrested" control experiments, the block length was 55 trials, and 40 of these trials followed the standard 4-epoch trial sequence: 10 with a 12° change and no stimulation, 10 with a 12° change and stimulation, 10 with no change and no stimulation, and 10 with no change and stimulation. For the remaining trials the sequence of epochs was stopped once the trial reached a particular benchmark: 5 stopped at one-patch, 5 stopped at visual pink noise, and 5 stopped at gray background. These sequence-arrested trials followed the same distance markers as the standard 4-epoch trial sequence, but without changing the content of the visual display at the transitions. Consequently, the overall length and the timing of stimulation on these control trials was matched to that on the normal trials. Because there was no opportunity for mice to earn rewards on these control trials, their fraction was kept low (15/55, 27%) to avoid losing motivation. We recorded 3–6 sessions in these experiments for each mouse to obtain at least 60 repetitions for each of the three types sequence-arrested trials. The experimenters were not blind to the genotype of animals, but the order of presentation for the different trial types in each experiment was randomized.

Fiber photometry—GCaMP photoexcitation and signal processing followed previous methods (Lerner et al., 2015), using a locked-in amplifier system (Tucker-Davis Technologies, Model RZ5D with Synapse software). The tissue was illuminated with a blue 465nm LED (Plexon) sinusoidally modulated at 211 Hz and a UV 405nm LED sinusoidally modulated at 531 Hz. The peak intensity of each LED was set to 20–30μW measured at the distal end of the patch cable. Both light sources were filtered through a fluorescence mixing cube (Doric Lens) and then coupled to an optic patch cable (NA 0.23, 200um core) that affixed to the optic cannula implanted in each mouse. The emitted fluorescent signal from GCaMP6f and the auto-fluorescence signal were collected by the same light pathway, and focused onto two femtowatt photoreceivers (Newport, model 2151). The photoreceiver output was routed to the RZ5D real-time signal processor, which extracted the fluorescent signal modulations due to the 465 and 405 nm excitation. The demodulated signals were then low-pass filtered (corner frequency of 15Hz) and routed to the data acquisition system.

We used two methods to calculate normalized GCaMP6f fluorescence signal (ΔF/F). In the first method, the UV auto-fluorescence signal was used as a control to correct possible artifacts. For each trial, the UV signal was transformed by linear regression to fit the raw

GCaMP6f signal. This fitted 405nm signal was then used to normalize the raw GCaMP6f signal as follows: ΔF/F = (465nm signal – fitted 405nm signal) / fitted 405nm signal. The second method used the median value of the 465nm signal from each trial to provide a baseline GCaMP6f signal. This baseline value was then used to normalize the 465nm signal as follows: ΔF/F = (465nm signal – median 465nm signal) / median 465nm signal. The second method produced the same trial-by-trial estimates as the first method, presumably because our head-fixed mice produced minimal artifacts, but the subtraction in the first method introduced higher ms-by-ms variance in the estimate. Consequently, the data presented in the paper were obtained with the second method. The onset timing of GCaMP transient aligned to either lick onset or visual change was defined as the time point at which the ΔF/F exceeded the 95% CI of the baseline (defined as the mean GCaMP signal in the 500-ms interval before the event) and remained above the 95% CI for at least 100 ms.

Histology—Mice were euthanized with CO_2 (1.0 LPM), after which they were transcardially perfused with ice-cold saline followed by phosphate buffered saline with 4% paraformaldehyde (PFA). Their brains were carefully removed and stored in the 4% PFA solution overnight, before they were transferred to the phosphate buffered saline with 20% sucrose solution for at least three days prior to sectioning. 50 μm frozen sections were cut coronally or sagittally using a freezing microtome, free-floating sections were processed for immunohistochemical labeling of GFP mounted on gelatin-coated glass slide and counterstained with a fluorescent blue counterstain. To visualize the injection site and axonal projections from viral transfected cells sections were imaged at 10x using a Zeiss fluorescent microscope using Neurolucida software (MBF Biosciences, Williston, VT) to produce a whole brain reconstruction from tiled images of coronal or sagittal sections.

QUANTIFICATION AND STATISTICAL ANALYSIS

All of the data were acquired and initially processed using custom scripts written in Matlab (The Mathworks, Natick, MA, USA).

Behavioral performance Analysis—For the psychometric data, results were pooled across sessions for each mouse to tabulate the overall lick probability for each amplitude of orientation change (including no change) separately for left and right visual fields and for with and without optogenetic stimulation. The lick probabilities were fitted with a cumulative Gaussian function using Psignifit3 (Wichmann and Hill, 2001). The fitted function had four parameters: mean, standard deviation of the Gaussian, bias (lower asymptote), and lapse rate (upper asymptote). Based on the standard deviation, we calculated the just-noticeable difference (JND), defined as the standard deviation multiplied by √2; the JND indicates the minimum change in signal strength that increases the detection rate by at least 50% of the available response range, once response bias and lapse rate have been taken into account. The same analysis also applied to the psychometric dataset sorted by running speed described below.

For experiments using a single value of orientation change, we also pooled across sessions to tabulate lick probability, and tabulated hit and false alarm rates based on the definitions of trial outcomes described for the behavioral tasks. Performance was then characterized by

measuring sensitivity (d') and criterion using methods from signal detection theory (Macmillan and Creelman, 2005), as follows: d' = Φ^{-1} (H) – Φ^{-1} (F), criterion = − (Φ^{-1} (H) + Φ^{-1} (F)/2, where Φ^{-1} is the inverse of normal cumulative distribution function, H is the hit rate and F is the false alarm rate. The 95% confidence intervals of d' and criterion were generated with bootstrapped resampling.

Running speed analysis—The instantaneous running speed was determined from the total number of pulses obtained from the optical encoder within each screen frame refresh (75Hz), taking into account the circumference of the running wheel. To divide psychometric data into speed quartiles, the mean running speed in the 500-ms interval before the change epoch was calculated for each trial. We divided the individual trials into quartiles based on the overall distributions of speeds within each session, and then pooled data across animals separately for each quartile to tabulate population psychometric curves based on the running speed. To quantify the influence of running speed on psychometric performance, we determined response bias, JND and lapse rate with bootstrapped resampling as described above for psychometric curve fitting. To quantify the effect of striatal stimulation on running speed during "sequence arrested" control trials, we pooled data across sessions to compute the time course of running speed for each mouse. The effect of stimulation on running speed was also summarized as the difference in speed between the baseline (mean in the 50-ms interval before stimulation) and the post-stimulation running speed (mean in the interval 50–100 ms after the stimulation offset).

Statistics—Statistical analyses were conducted in Matlab using the statistics and machine learning toolbox and Prism 7 (GraphPad), and statistical significance was accepted for $p<0.05$. Two-way ANOVAs were used to assess the interaction between optogenetic stimulation and spatial location of expected visual change on response bias and sensitivity, using (stimulation vs no stimulation) and (contralateral vs ipsilateral) as two independent factors, the interactions were further tested with *post hoc* multiple comparisons using Bonferroni methods. On-way ANOVAs were used assess contribution of running speed on psychometric performance, as well as running speed on the stimulation induced performance change. Paired sample t-tests were used to compare the within-subject effect of optogenetic stimulation on response bias and sensitivity, unless otherwise specifically stated in the text. Paired sample non-parametric Wilcoxon sign rank tests were performed to compare the within-subject effect of optogenetic stimulation on response latency for the chronometric data, as well as within subject effect of stimulation on running speed. Non-parametric Wilcoxon rank sum tests were performed to compare the effect of optogenetic stimulation between two visual sides for each trial number in the time course analysis, and to compare psychometric performance between fastest and slowest speed quartiles. One sample t-test were used to compare whether the choice-related GCaMP6f signal across subjects was significantly from zero. The value of n reported in the figures and results indicates the number of animals. Error bars in figures indicate 95% confidence interval of the median or mean, unless indicated otherwise.

DATA AVAILABILITY

The data that support the findings of this study will be made available from the corresponding author upon reasonable request.

Supplementary Material

Refer to Web version on PubMed Central for supplementary material.

Acknowledgments

The authors thank Drs. Kravitz and Krashes for their advice, and N. Nichols and T. Ruffner for technical support. This work was supported by the National Eye Institute Intramural Research Program at the National Institutes of Health.

References

Albin RL, Young AB, Penney JB. The functional anatomy of basal ganglia disorders. Trends Neurosci. 1989; 12:366–375. [PubMed: 2479133]

Bogacz R. Optimal decision-making theories: linking neurobiology with behaviour. Trends in Cognitive Sciences. 2007; 11:118–125. [PubMed: 17276130]

Bogacz R, Gurney K. The basal ganglia and cortex implement optimal decision making between alternative actions. Neural Comput. 2007; 19:442–477. [PubMed: 17206871]

Botha H, Carr J. Attention and visual dysfunction in Parkinson's disease. Parkinsonism Relat Disord. 2012; 18:742–747. [PubMed: 22503538]

Brainard DH. The Psychophysics Toolbox. Spat Vis. 1997; 10:433–436. [PubMed: 9176952]

Brown LL, Schneider JS, Lidsky TI. Sensory and cognitive functions of the basal ganglia. Curr Opin Neurobiol. 1997; 7:157–163. [PubMed: 9142758]

Cui G, Jun SB, Jin X, Pham MD, Vogel SS, Lovinger DM, Costa RM. Concurrent activation of striatal direct and indirect pathways during action initiation. Nature. 2013; 494:238–242. [PubMed: 23354054]

DeLong MR. Primate models of movement disorders of basal ganglia origin. Trends in NeuroSciences. 1990; 13:281–285. [PubMed: 1695404]

Ding L, Gold JI. The Basal Ganglia's Contributions to Perceptual Decision Making. Neuron. 2013; 79:640–649. [PubMed: 23972593]

Ding L, Gold JI. Separate, Causal Roles of the Caudate in Saccadic Choice and Execution in a Perceptual Decision Task. Neuron. 2012; 75:865–874. [PubMed: 22958826]

Ding L, Gold JI. Caudate encodes multiple computations for perceptual decisions. J Neurosci. 2010; 30:15747–15759. [PubMed: 21106814]

Dudman JT, Krakauer JW. The basal ganglia: from motor commands to the control of vigor. Curr Opin Neurobiol. 2016; 37:158–166. [PubMed: 27012960]

Eastman KM, Huk AC. PLDAPS: A Hardware Architecture and Software Toolbox for Neurophysiology Requiring Complex Visual Stimuli and Online Behavioral Control. Front Neuroinform. 2012; 6:1. [PubMed: 22319490]

Forstmann BU, Anwander A, Schäfer A, Neumann J, Brown S, Wagenmakers EJ, Bogacz R, Turner R. Cortico-striatal connections predict control over speed and accuracy in perceptual decision making. Proc Natl Acad Sci USA. 2010; 107:15916–15920. [PubMed: 20733082]

Forstmann BU, Dutilh G, Brown S, Neumann J, von Cramon DY, Ridderinkhof KR, Wagenmakers E-J. Striatum and pre-SMA facilitate decision-making under time pressure. Proc Natl Acad Sci USA. 2008; 105:17538–17542. [PubMed: 18981414]

Gerfen CR, Engber TM, Mahan LC, Susel Z, Chase TN, Monsma FJ, Sibley DR. D1 and D2 dopamine receptor-regulated gene expression of striatonigral and striatopallidal neurons. Science. 1990; 250:1429–1432. [PubMed: 2147780]

Gerfen CR, Paletzki R, Heintz N. GENSAT BAC cre-recombinase driver lines to study the functional organization of cerebral cortical and basal ganglia circuits. Neuron. 2013; 80:1368–1383. [PubMed: 24360541]

Gerfen CR, Surmeier DJ. Modulation of striatal projection systems by dopamine. Annu Rev Neurosci. 2011; 34:441–466. [PubMed: 21469956]

Glickfeld LL, Histed MH, Maunsell JHR. Mouse primary visual cortex is used to detect both orientation and contrast changes. J Neurosci. 2013; 33:19416–19422. [PubMed: 24336708]

Gold JI, Shadlen MN. The neural basis of decision making. Annu Rev Neurosci. 2007; 30:535–574. [PubMed: 17600525]

Gurney K, Prescott TJ, Redgrave P. A computational model of action selection in the basal ganglia. I. A new functional anatomy. Biol Cybern. 2001; 84:401–410. [PubMed: 11417052]

Haber SN, Kim KS, Mailly P, Calzavara R. Reward-related cortical inputs define a large striatal region in primates that interface with associative cortical connections, providing a substrate for incentive-based learning. J Neurosci. 2006; 26:8368–8376. [PubMed: 16899732]

Hikosaka O, Kim HF, Yasuda M, Yamamoto S. Basal ganglia circuits for reward value-guided behavior. Annu Rev Neurosci. 2014; 37:289–306. [PubMed: 25032497]

Hikosaka O, Takikawa Y, Kawagoe R. Role of the basal ganglia in the control of purposive saccadic eye movements. Physiol Rev. 2000; 80:953–978. [PubMed: 10893428]

Hikosaka O, Wurtz RH. Modification of saccadic eye movements by GABA-related substances. I. Effect of muscimol and bicuculline in monkey superior colliculus. J Neurophysiol. 1985a; 53:266–291. [PubMed: 2983037]

Hikosaka O, Wurtz RH. Modification of saccadic eye movements by GABA-related substances. II. Effects of muscimol in monkey substantia nigra pars reticulata. J Neurophysiol. 1985b; 53:292–308. [PubMed: 2983038]

Hintiryan H, Foster NN, Bowman I, Bay M, Song MY, Gou L, Yamashita S, Bienkowski MS, Zingg B, Zhu M, Yang XW, Shih JC, Toga AW, Dong HW. The mouse cortico-striatal projectome. Nat Neurosci. 2016; 19:1100–1114. [PubMed: 27322419]

Ivanoff J, Branning P, Marois R. fMRI evidence for a dual process account of the speed-accuracy tradeoff in decision-making. PLoS ONE. 2008; 3:e2635. [PubMed: 18612380]

Jin X, Tecuapetla F, Costa RM. Basal ganglia subcircuits distinctively encode the parsing and concatenation of action sequences. Nat Neurosci. 2014; 17:423–430. [PubMed: 24464039]

Kim HF, Amita H, Hikosaka O. Indirect Pathway of Caudal Basal Ganglia for Rejection of Valueless Visual Objects. Neuron. 2017; 94:920–930. [PubMed: 28521141]

Kim HF, Hikosaka O. Distinct basal ganglia circuits controlling behaviors guided by flexible and stable values. Neuron. 2013; 79:1001–1010. [PubMed: 23954031]

Kravitz AV, Freeze BS, Parker PRL, Kay K, Thwin MT, Deisseroth K, Kreitzer AC. Regulation of parkinsonian motor behaviours by optogenetic control of basal ganglia circuitry. Nature. 2010; 466:622–626. [PubMed: 20613723]

Lau B, Glimcher PW. Value representations in the primate striatum during matching behavior. Neuron. 2008; 58:451–463. [PubMed: 18466754]

Lauwereyns J, Takikawa Y, Kawagoe R, Kobayashi S, Koizumi M, Coe B, Sakagami M, Hikosaka O. Feature-Based Anticipation of Cues that Predict Reward in Monkey Caudate Nucleus. Neuron. 2002a; 33:463–473. [PubMed: 11832232]

Lauwereyns J, Watanabe K, Coe B, Hikosaka O. A neural correlate of response bias in monkey caudate nucleus. Nature. 2002b; 418:413–417. [PubMed: 12140557]

Lerner TN, Shilyansky C, Davidson TJ, Evans KE, Beier KT, Zalocusky KA, Crow AK, Malenka RC, Luo L, Tomer R, Deisseroth K. Intact-Brain Analyses Reveal Distinct Information Carried by SNc Dopamine Subcircuits. Cell. 2015; 162:635–647. [PubMed: 26232229]

Lo CC, Wang XJ. Cortico-basal ganglia circuit mechanism for a decision threshold in reaction time tasks. Nat Neurosci. 2006; 9:956–963. [PubMed: 16767089]

Macmillan, NA., Creelman, CD. Detection Theory: A User's Guide. 2. Lawrence Erlbaum Associates; 2005.

Mazzoni P, Hristova A, Krakauer JW. Why don“t we move faster? Parkinson”s disease, movement vigor, and implicit motivation. J Neurosci. 2007; 27:7105–7116. [PubMed: 17611263]

Mink JW. The Basal Ganglia and involuntary movements: impaired inhibition of competing motor patterns. Arch Neurol. 2003; 60:1365–1368. [PubMed: 14568805]

Nambu A, Tokuno H, Takada M. Functional significance of the cortico-subthalamo-pallidal “hyperdirect” pathway. Neurosci Res. 2002; 43:111–117. [PubMed: 12067746]

Niell CM, Stryker MP. Modulation of visual responses by behavioral state in mouse visual cortex. Neuron. 2010; 65:472–479. [PubMed: 20188652]

Paxinos, G., Franklin, K. The mouse brain in stereotaxic coordinates. 2004.

Pelli DG. The VideoToolbox software for visual psychophysics: transforming numbers into movies. Spat Vis. 1997; 10:437–442. [PubMed: 9176953]

Poort J, Khan AG, Pachitariu M, Nemri A, Orsolic I, Krupic J, Bauza M, Sahani M, Keller GB, Mrsic-Flogel TD, Hofer SB. Learning Enhances Sensory and Multiple Non-sensory Representations in Primary Visual Cortex. Neuron. 2015; 86:1478–1490. [PubMed: 26051421]

Prusky GT, Alam NM, Beekman S, Douglas RM. Rapid quantification of adult and developing mouse spatial vision using a virtual optomotor system. Invest Ophthalmol Vis Sci. 2004; 45:4611–4616. [PubMed: 15557474]

Ratcliff R, Smith PL. A Comparison of Sequential Sampling Models for Two-Choice Reaction Time. Psychological Review. 2004; 111:333. [PubMed: 15065913]

Reig R, Silberberg G. Distinct Corticostriatal and Intracortical Pathways Mediate Bilateral Sensory Responses in the Striatum. Cerebral Cortex. 2016; 26:4405–4415. [PubMed: 27664965]

Reig R, Silberberg G. Multisensory integration in the mouse striatum. Neuron. 2014; 83:1200–1212. [PubMed: 25155959]

Reimer J, Froudarakis E, Cadwell CR, Yatsenko D, Denfield GH, Tolias AS. Pupil fluctuations track fast switching of cortical states during quiet wakefulness. Neuron. 2014; 84:355–362. [PubMed: 25374359]

Roitman JD, Shadlen MN. Response of neurons in the lateral intraparietal area during a combined visual discrimination reaction time task. J Neurosci. 2002; 22:9475–9489. [PubMed: 12417672]

Samejima K, Ueda Y, Doya K, Kimura M. Representation of action-specific reward values in the striatum. Science. 2005; 310:1337–1340. [PubMed: 16311337]

Schmucker C, Seeliger M, Humphries P, Biel M, Schaeffel F. Grating acuity at different luminances in wild-type mice and in mice lacking rod or cone function. Invest Ophthalmol Vis Sci. 2005; 46:398–407. [PubMed: 15623801]

Selemon LD, Goldman-Rakic PS. Longitudinal topography and interdigitation of corticostriatal projections in the rhesus monkey. The Journal of Neuroscience. 1985; 5:776–794. [PubMed: 2983048]

Shadlen MN, Kiani R. Decision making as a window on cognition. Neuron. 2013; 80:791–806. [PubMed: 24183028]

Sinex DG, Burdette LJ, Pearlman AL. A psychophysical investigation of spatial vision in the normal and reeler mutant mouse. Vision Research. 1979; 19:853–857. [PubMed: 516456]

Sippy T, Lapray D, Crochet S, Petersen CCH. Cell-Type-Specific Sensorimotor Processing in Striatal Projection Neurons during Goal-Directed Behavior. Neuron. 2015; 88:298–305. [PubMed: 26439527]

Sutton, RS., Barto, AG. Reinforcement Learning. MIT Press; 1998.

Tai LH, Lee AM, Benavidez N, Bonci A, Wilbrecht L. Transient stimulation of distinct subpopulations of striatal neurons mimics changes in action value. Nat Neurosci. 2012; 15:1281–1289. [PubMed: 22902719]

Tecuapetla F, Jin X, Lima SQ, Costa RM. Complementary Contributions of Striatal Projection Pathways to Action Initiation and Execution. Cell. 2016; 166:703–715. [PubMed: 27453468]

Tecuapetla F, Matias S, Dugue GP, Mainen ZF, Costa RM. Balanced activity in basal ganglia projection pathways is critical for contraversive movements. Nat Commun. 2014; 5:4315. [PubMed: 25002180]

Thura D, Cisek P. The Basal Ganglia Do Not Select Reach Targets but Control the Urgency of Commitment. Neuron. 2017; 95:1160–1170. [PubMed: 28823728]

Turner RS, Desmurget M. Basal ganglia contributions to motor control: a vigorous tutor. Curr Opin Neurobiol. 2010; 20:704–716. [PubMed: 20850966]

van Veen V, Krug MK, Carter CS. The neural and computational basis of controlled speed-accuracy tradeoff during task performance. J Cogn Neurosci. 2008; 20:1952–1965. [PubMed: 18416686]

Vrtunski P, Wolin LR. Measurement of licking response execution in the rat. Physiol Behav. 1974; 12:881–886. [PubMed: 4837425]

Wall NR, De La Parra M, Callaway EM, Kreitzer AC. Differential innervation of direct- and indirect-pathway striatal projection neurons. Neuron. 2013; 79:347–360. [PubMed: 23810541]

Weijnen JA. Licking behavior in the rat: measurement and situational control of licking frequency. Neurosci Biobehav Rev. 1998; 22:751–760. [PubMed: 9809310]

Wichmann FA, Hill NJ. The psychometric function: I. Fitting, sampling, and goodness of fit. Percept Psychophys. 2001; 63:1293–1313. [PubMed: 11800458]

Wu Y, Richard S, Parent A. The organization of the striatal output system: a single-cell juxtacellular labeling study in the rat. Neurosci Res. 2000; 38:49–62. [PubMed: 10997578]

Yamamoto S, Monosov IE, Yasuda M, Hikosaka O. What and where information in the caudate tail guides saccades to visual objects. J Neurosci. 2012; 32:11005–11016. [PubMed: 22875934]

Highlights

- Activation of basal ganglia biases perceptual choices in a visual detection task
- Direct pathway stimulation biases choices in favor of expected contralateral events
- Effects on perceptual choice require the presence of task-relevant visual stimuli
- Choice-related GCaMP activity also requires the presence of task-relevant stimuli

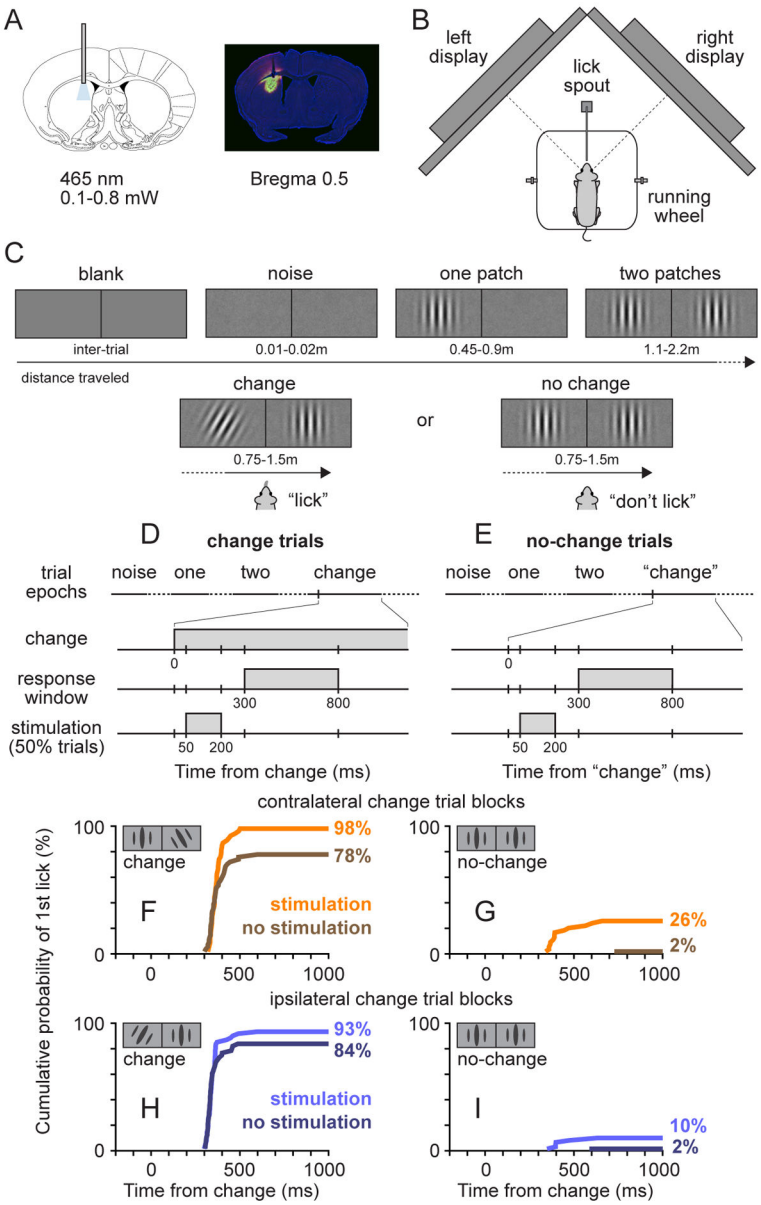

Figure 1. Visual orientation-change detection task and examples of behavioral performance

(A) Localization of optogenetic stimulation in striatum. Left: stereotaxic placement of fiber and optogenetic stimulation. Right: coronal section from example Drd1a-cre mouse, showing viral expression in dorsomedial striatum and placement of optical fiber. (B) Top-down view of the behavioral apparatus, showing a head-fixed mouse on the polystyrene wheel viewing left and right visual displays. (C) Sequence of visual epochs during the task, illustrating a trial during left change blocks. The length of each epoch was measured by the distance traveled on the wheel. (D–E) Timeline of events during change (D) and no-change trials (E) interleaved in the block. The outcome of a trial was determined by whether the first lick fell within the 500ms response window starting 300 ms after the stimulus change. The 150ms optogenetic stimulation ended before the onset of the response window. (F–I) Cumulative lick probabilities from an example session in one Drd1a-cre mouse, divided to

illustrate the 8 possible trial types. A 12° orientation change was used in this session, and only the timing of the first lick made by the mouse on each trial was used for quantification, aligned to the onset of the change epoch. Data are from the same mouse as shown in panel A (right).

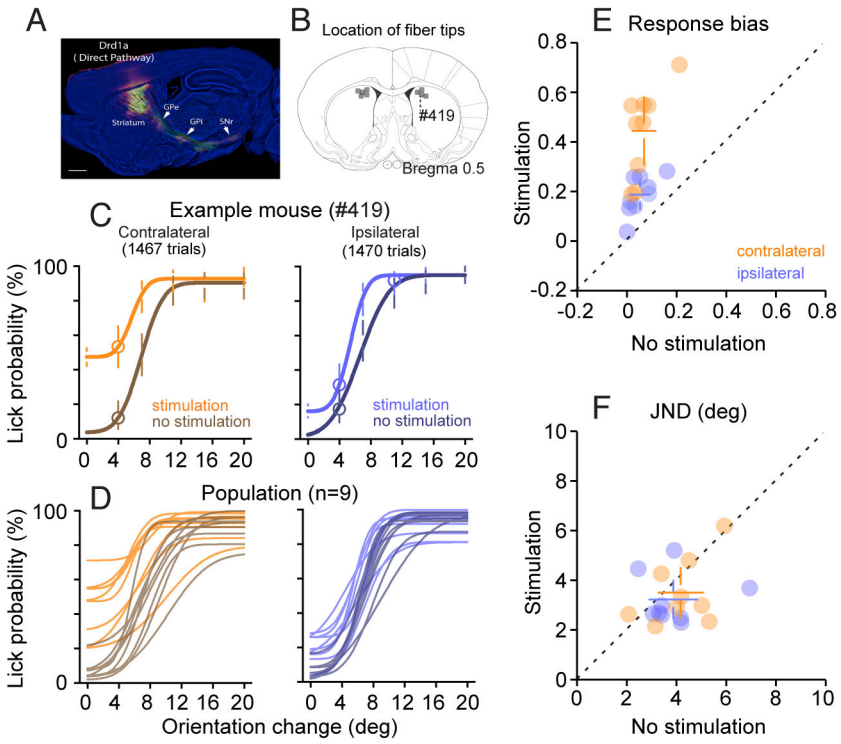

Figure 2. Optogenetic activation of the direct pathway increased response bias preferentially for visual events on the contralateral side

(A) Sagittal section of an example Drd1a mouse, showing Cre-dependent viral expression in the striatum and downstream axonal targets of transfected neurons (GPi, SNr and GPe). Scale bar,1mm. Yellow: YFP, magenta: anti-GFP/YFP antibody staining. (B) Summary of unilateral optic fiber tip placements in the striatum of all the Drd1a-cre used in the study (grey dots). The number label indicates the tip placement for the example mouse whose data are shown in C. (C) Psychometric data of an example Drd1a-cre mice. Circles show lick probability pooled across sessions for each orientation change tested. Smooth curves show fitted cumulative Gaussian function. Error bars show 95% confidence interval. Left: psychometric data for orientation change contralateral to the optic fiber implant, with (orange) and without (brown) optical stimulation. Right: psychometric data for orientation change ipsilateral to the optic fiber implant, with (light blue) and without (dark blue) optical stimulation. (D) Fitted psychometric curves from all Drd1a mice (n=9); each curve is from one mouse. Left: psychometric curves for performance during blocks containing contralateral visual events, with (orange) and without (brown) stimulation. Right: psychometric curves during blocks with ipsilateral visual events, with (light blue) and without (dark blue) stimulation. (E) Comparison of response biases from psychometric curves with and without dMSN stimulation, during blocks containing contralateral (orange) and ipsilateral (blue) visual events. Filled circles are data from each mouse, open circles represent population average. Error bars are 95% CI. (F) Comparison of JNDs from psychometric curves with and without dMSN stimulation. See also Figure S1.

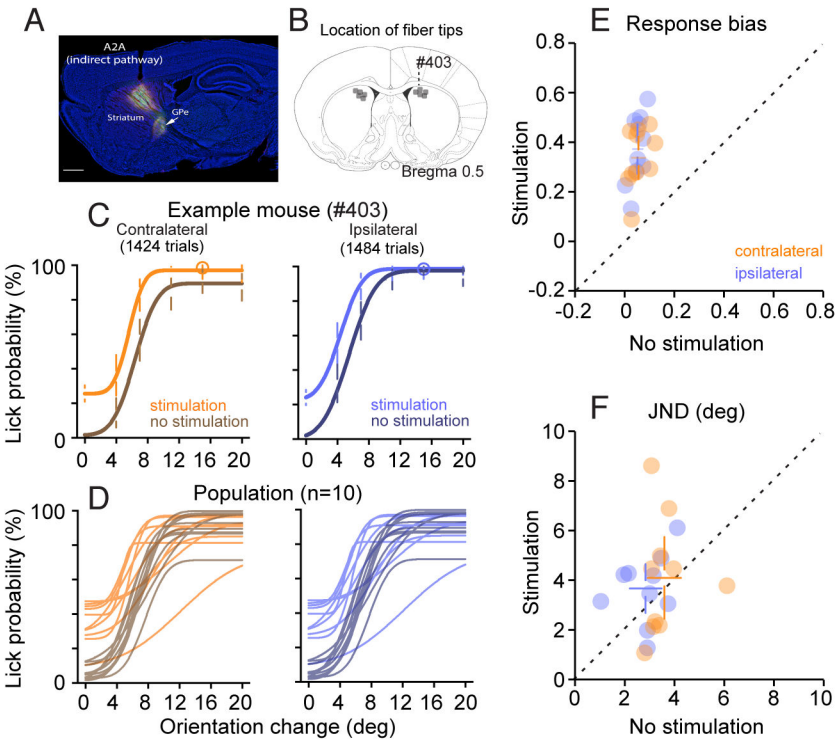

Figure 3. Optogenetic activation of the indirect pathway increased response bias equally for visual events in either visual hemifield

(A) Sagittal section of an example A2a mouse, showing Cre-dependent viral expression in the striatum and downstream axonal targets of transfected neurons (GPe only). Scale bar, 1mm. Yellow: YFP, magenta: anti-GFP/YFP antibody staining. (B) Summary of unilateral optic fiber tip placements for all A2a-cre mice used in the study (grey dots). Number label indicates the tip placement for the example mouse whose data are shown in C. (C) Psychometric data of an example A2a-cre mice. (D) Fitted psychometric curves from all A2a-cre mice (n=10). (E) Comparison of response biases from psychometric curves with and without iMSN stimulation. (F) Comparison of JNDs from psychometric curves with and without iMSN stimulation. Other conventions same as in Figure 2.

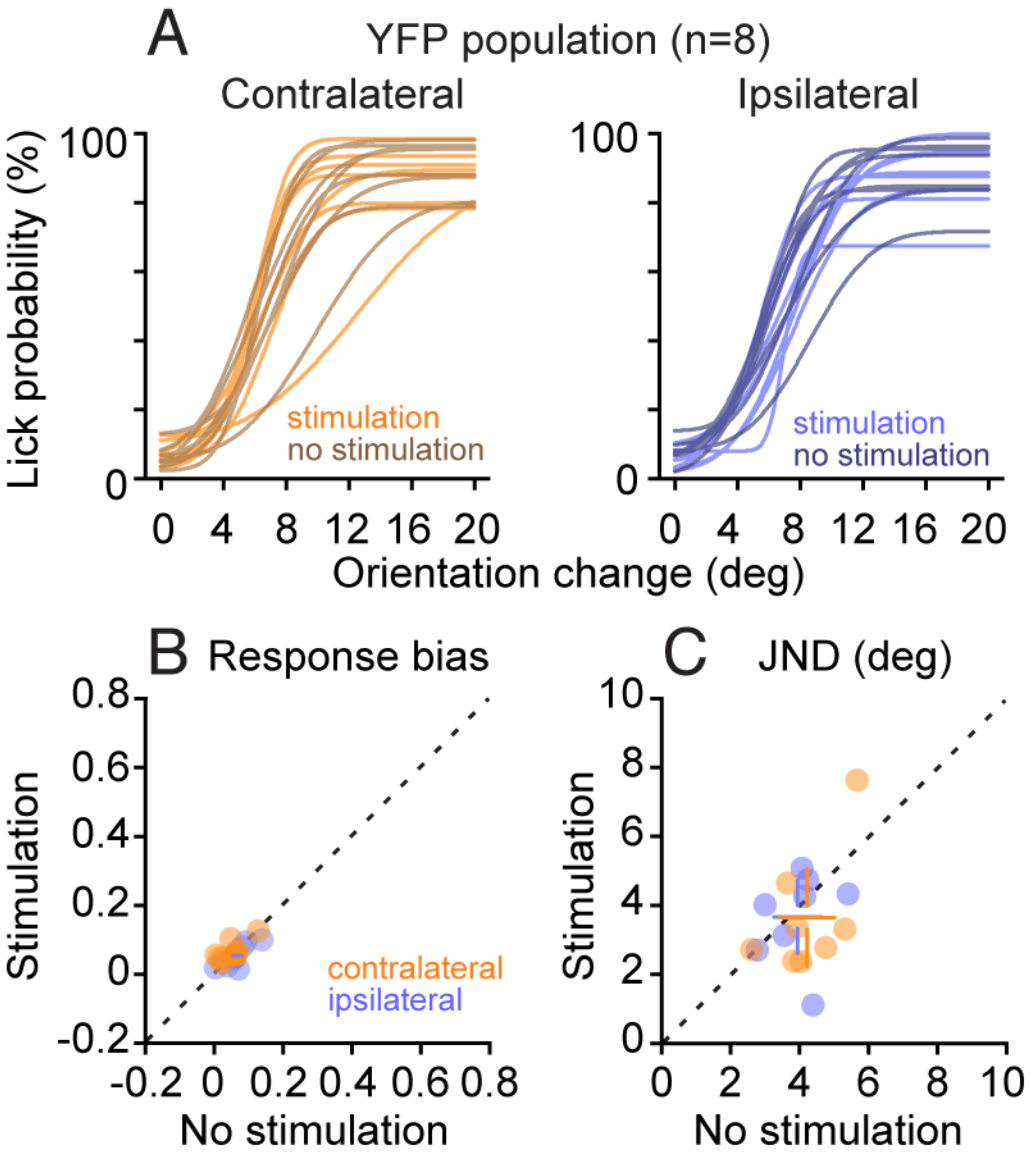

Figure 4. Optical stimulation in YFP control mice did not change psychophysical performance

(A) Population summary of psychometric curves with and without optical stimulation from all 8 mice injected with eYFP virus. (B) Comparison of response biases from psychometric curves with and without optical stimulation. (C) Comparison of JNDs from psychometric curves with and without optical stimulation. Other conventions same as in Figure 2.

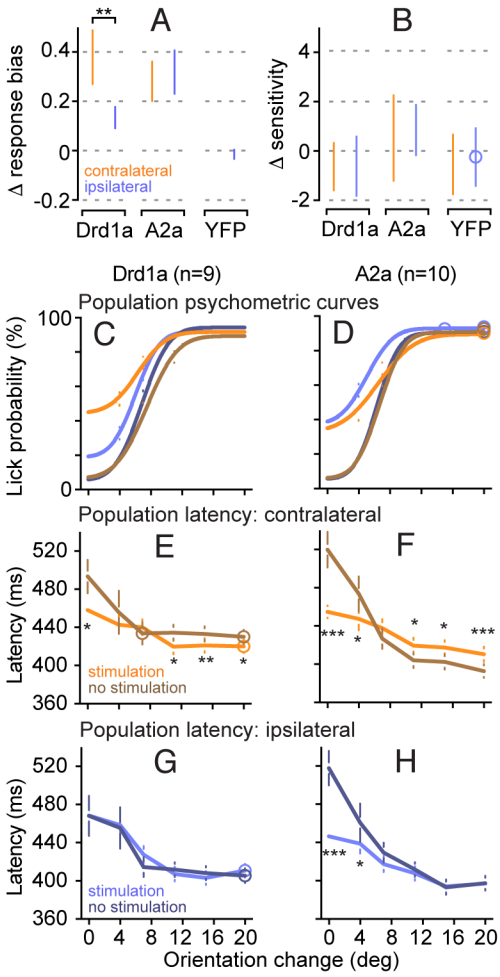

Figure 5. Summary of psychophysical performance with and without striatal optogenetic stimulation

(A) Comparison of striatal stimulation effects on response bias in Drd1a-cre, A2a-cre and YFP mice, defined as response bias with stimulation minus response bias without stimulation. (B) Comparison of striatal stimulation effects on JND in all three genotypes, defined as JND with stimulation minus JND without stimulation. (C) Mean psychometric curves obtained by pooling data across all 9 Drd1a mice, separately for contralateral and ipsilateral blocks, and with and without striatal stimulation. (D) Mean psychometric curves from all 10 A2a mice. (E) Chronometric curves of response latency for contralateral visual changes with and without striatal stimulation, pooled across all Drd1a mice. (F) Chronometric curves of response latency for contralateral visual changes, pooled across all A2a mice. (G) Chronometric curves for ipsilateral visual changes from Drd1a mice. (H) Chronometric curves for ipsilateral visual changes from A2a mice. Error bars are median ± 95% CI. ***p<0.001, **p<0.01, *p<0.05. See also Figures S2-S5.

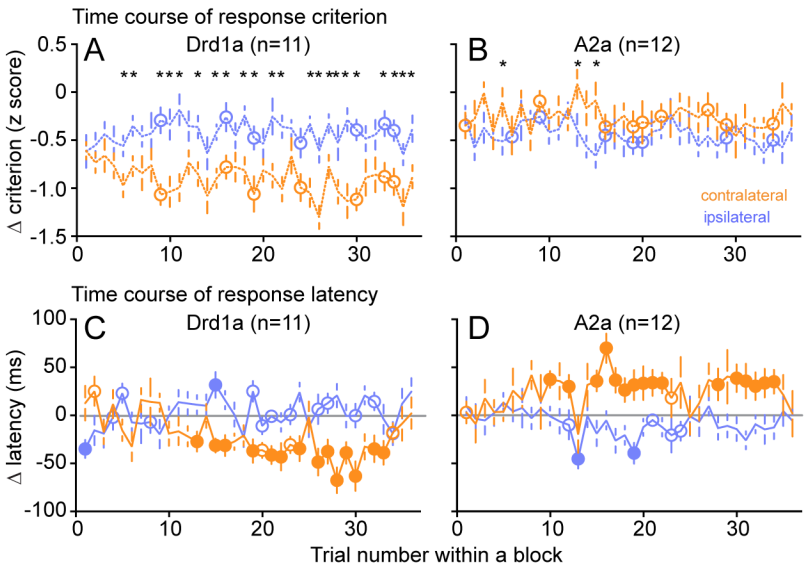

Figure 6. Effects of striatal stimulation on response criterion and latency emerged after a few trials within a block

(A) Effects on response criterion caused by dMSN stimulation plotted as a function of trial number during a block. Change in criterion (defined as stimulation minus no stimulation) shown separately for blocks containing contralateral (orange) or ipsilateral (blue) 12° orientation chan ges. Each open circle shows the population median (n=11) of the induced changes for that trial number in the block. Error bar: SEM. The symbol (*) indicates a significant difference ($p<0.05$, Wilcoxon rank sum test) between contralateral and ipsilateral values. (B) Time course of changes in response criterion caused by iMSN stimulation. (C–D) Time course of changes in response latency caused by dMSN (C) or iMSN (D) stimulation.

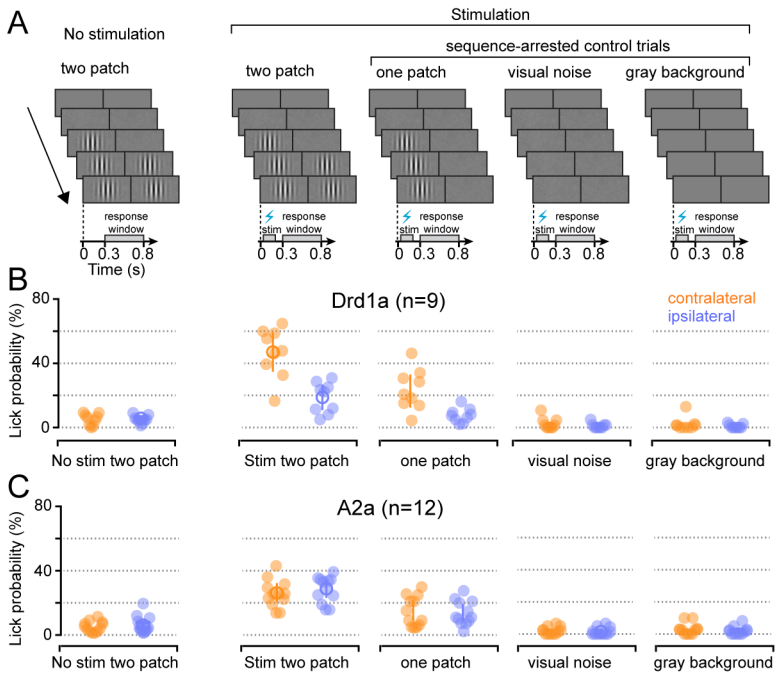

Figure 7. Changes in performance caused by striatal stimulation depended on the presence of behaviorally relevant visual stimuli

(A) Schematics of visual displays and timing of optogenetic stimulation in sequence-arrested control trials and normal no-change (‘two-patch’) trials. All sequence-arrested control trials had optical stimulation at a distance equivalent to normal trials, and were interleaved with 12° cha nge and no-change trials. (B) Lick probability during response window observed across different conditions in Drd1a-cre mice when visual event could occur in contralateral (orange) and ipsilateral (blue) hemifield. Filled circles represent data from individual mice, open circles show population mean. Error bars are 95% CI. (C) Lick probability during response window observed across different conditions in A2a-cre mice.

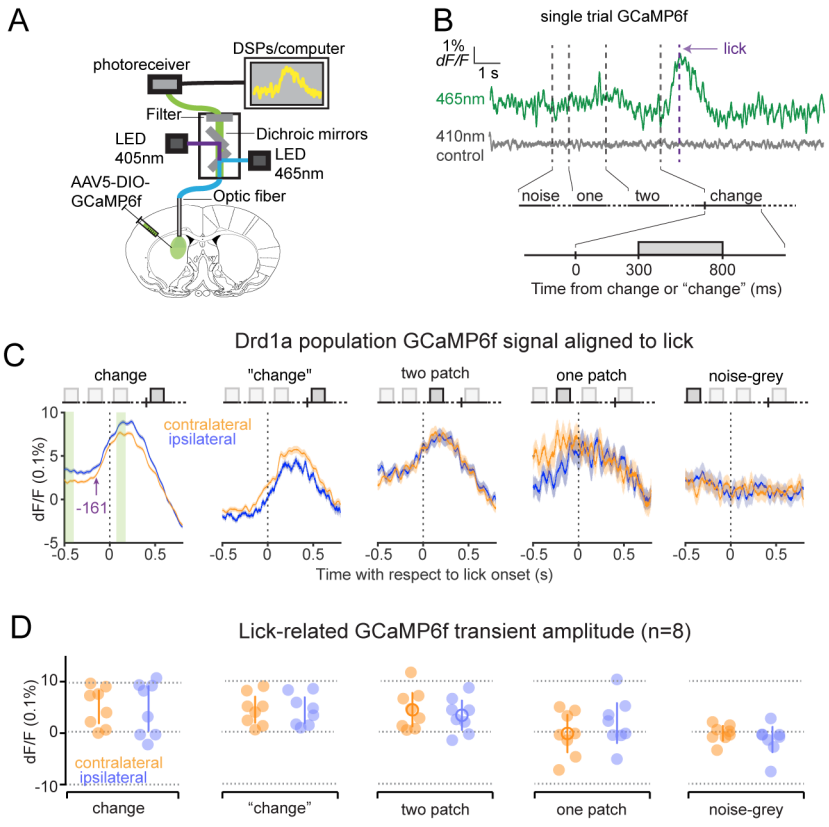

Figure 8. Lick-related Ca^{2+} transients in dMSNs occurred only when behaviorally relevant visual stimuli were present

(A) Diagram of fiber photometry setup to record population GCaMP6f signals in striatal dMSNs. (B) ΔF/F traces of GCaMP6f signals (green, 465nm) and autofluorescence (grey, 405nm) from an example trial containing a hit response. Vertical lines (grey) indicate onset of each epoch and the onset of the first lick (purple). (C) Time course of normalized population mean (n=8) GCaMP6f signals aligned to lick onset during different epochs when visual event could occur in contralateral (orange) or ipsilateral (blue) hemifield. Thick lines represent mean and shading indicates SEM. Light green stripes in left panel indicate 100ms time windows used to calculate the amplitude of GCaMP6f transients in panel D, purple arrow indicates time of mean onset of lick-related GCaMP6f transients (−161 ms). (D) Amplitude of lick-related GCaMP6f transient during different visual epochs. Each filled circle shows data from one mouse, open circles are population mean, and error bars indicate SEM. See also Figure S6.